Acta Crystallographica Section D
Biological Crystallography
ISSN 0907-4449

Structural plasticity of tubulin assembly probed by vinca-domain ligands

Fanomezana M. Ranaivoson,[a] Benoît Gigant,[a]* Simon Berritt,[b] Madeleine Joullié[b] and Marcel Knossow[a]*

[a]Laboratoire d'Enzymologie et Biochimie Structurales, Centre de Recherche de Gif, CNRS, 91198 Gif-sur-Yvette, France, and [b]Department of Chemistry, University of Pennsylvania, 231 South 34th Street, Philadelphia, PA 19104, USA

Correspondence e-mail: gigant@lebs.cnrs-gif.fr, knossow@lebs.cnrs-gif.fr

Received 16 December 2011
Accepted 18 April 2012

PDB References:
sT_2R–ustiloxin D, 3ut5; sT_2R–vinblastine, 4eb6.

Vinca-domain ligands are compounds that bind to tubulin at its inter-heterodimeric interface and favour heterogeneous protofilament-like assemblies, giving rise to helices and rings. This is the basis for their inhibition of microtubule assembly, for their antimitotic activities and for their use in anticancer chemotherapy. Ustiloxins are vinca-domain ligands with a well established total synthesis. A 2.7 Å resolution structure of ustiloxin D bound to the vinca domain embedded in the complex of two tubulins with the stathmin-like domain of RB3 (T_2R) has been determined. This finding precisely defines the interactions of ustiloxins with tubulin and, taken together with structures of other vinca-ligand complexes, allows structure-based suggestions to be made for improved activity. These comparisons also provide a rationale for the large-scale polymorphism of the protofilament-like assemblies mediated by vinca-domain ligands based on local differences in their interactions with the two tubulin heterodimers constituting their binding site.

1. Introduction

Microtubules (MTs) are dynamic protein assemblies that are used to move and organize cellular components for processes such as cell morphogenesis, membrane trafficking and cell division. They are constituted of straight and parallel protofilaments which interact laterally and roll to form a 25 nm diameter hollow cylinder. Each protofilament is assembled in a head-to-tail fashion from $\alpha\beta$-tubulin heterodimers (tubulin). The molecules in a protofilament are said to interact longitudinally. As tubulin is the major constituent of the mitotic spindle, it is the target of antimitotic compounds that affect microtubule dynamics and arrest cell division. Many of these compounds interact with soluble tubulin and prevent its assembly into MTs by binding at the longitudinal interface between tubulin subunits. By doing so, they force the subunits into a curved assembly and prevent the formation of straight microtubular protofilaments. Depending on their binding site, these agents fall into two families that are named according to a prototypical ligand. Compounds in the colchicine group bind at the interface of the two subunits of a heterodimer (Dorléans *et al.*, 2009), whereas those in the vinblastine group (Fig. 1) target the interdimeric interface of two heterodimers. Ligands in the second group promote the isodesmic association of tubulin in protofilament-like assemblies, mostly rings and helices of various sizes (Amos *et al.*, 1984; Mitra & Sept, 2004). Their sites define what has been termed the vinca domain. In addition to vinblastine (Fig. 1*a*), they comprise structurally different molecules including depsipeptides and peptides (Hamel, 1992; Hamel & Covell, 2002) which may be linear,

as in dolastatins and their derivatives, or heterocyclic, as in cryptophycins, phomopsins (Fig. 1*b*) and ustiloxins.

Ustiloxins were originally isolated from the fungus *Ustilaginoidea virens*, a parasite of rice plants (Koiso *et al.*, 1992). They consist of a 13-membered macrocycle involving C atoms at positions 11 and 13 (Fig. 1*c*), with a chiral tertiary aryl–alkyl ether linkage at position 13, a feature which relates ustiloxins to phomopsins (Fig. 1*b*). Ustiloxin D is one of the simplest examples of this group of compounds (Fig. 1*c*). Chemical variations in natural ustiloxins are defined by the group at the phenol position *para* to the ether bond (position 16 in Fig. 1*c*) and by that at position 6 of the macrocycle. A total synthesis of ustiloxins has been reported, as well as a structure–activity study of ustiloxin D analogues in which the efficiencies of microtubule polymerization inhibition were compared (Joullié *et al.*, 2011; Li *et al.*, 2008). Structures of tubulin–ustiloxin complexes would allow these results to be rationalized and might suggest ustiloxin modifications that would yield more active compounds. The assembly of two tubulins held in a curved protofilament-like arrangement by the stathmin-like domain of the RB3 protein (T_2R; Ravelli *et al.*, 2004) provides a suitable platform for the study of vinca-domain ligands as it comprises an assembled domain at the interface of its two constitutive tubulins (Cormier *et al.*, 2008; Gigant *et al.*, 2005). Recently, changes in the preparation of the complex which include the limited proteolysis of tubulin by subtilisin (the resulting complex is notated sT_2R) have yielded a crystal form that diffracts to close to 2 Å resolution (Nawrotek *et al.*, 2011), a significant improvement compared with the 3.5 Å resolution limit of the previously available crystals.

Here, we report the 2.7 Å resolution structure of the complex of ustiloxin D with subtilisin-treated tubulin within T_2R, which defines the tubulin residues interacting with ustiloxin D as well as the conformational changes induced by the ligand within each subunit. This allows us to address two important aspects of the structure–activity relationships of vinca-domain ligands: firstly, the effects of substitutions on the interaction of ustiloxins with tubulin and, secondly, the influence of vinca-domain ligands on the tubulin oligomers that form in their presence.

2. Materials and methods

2.1. Tubulin-complex preparation

Sheep brain tubulin was purified by two cycles of polymerization in a high-molarity buffer followed by depolymerization (Castoldi & Popov, 2003) and was stored in 50 m*M* potassium MES pH 6.8, 33% glycerol, 0.25 m*M* $MgCl_2$, 0.5 m*M* EGTA, 0.1 m*M* GTP in liquid nitrogen until use. Before preparation of complexes with the RB3 stathmin-like domain, an additional microtubule assembly/disassembly cycle was performed. Tubulin concentrations were deduced from its absorbance (ε_{278} = 1.2 ml cm^{-1} mg^{-1}), assuming that the molecular mass of the heterodimer was 100 kDa (Correia *et al.*, 1987). The RB3 stathmin-like domain double mutant (Cys14Ala and Phe20Trp; stathmin numbering; Charbaut *et al.*, 2001) was expressed and purified as described previously (Dorléans *et al.*, 2007); its concentration was determined from its absorption at 280 nm. To produce the sT_2R complexes, the C-termini of α- and β-tubulins were removed by subtilisin treatment (Knipling *et al.*, 1999). Briefly, tubulin was incubated with subtilisin (Sigma) at 1%(*w*/*w*) for 20 min at 298 K and proteolysis was stopped by adding phenylmethylsulfonyl fluoride at 0.1%(*w*/*v*). The RB3 stathmin-like domain was added to subtilisin-treated tubulin in a 1.3:2 molar ratio and the resulting sample was concentrated to 15–20 mg ml^{-1} for crystallization.

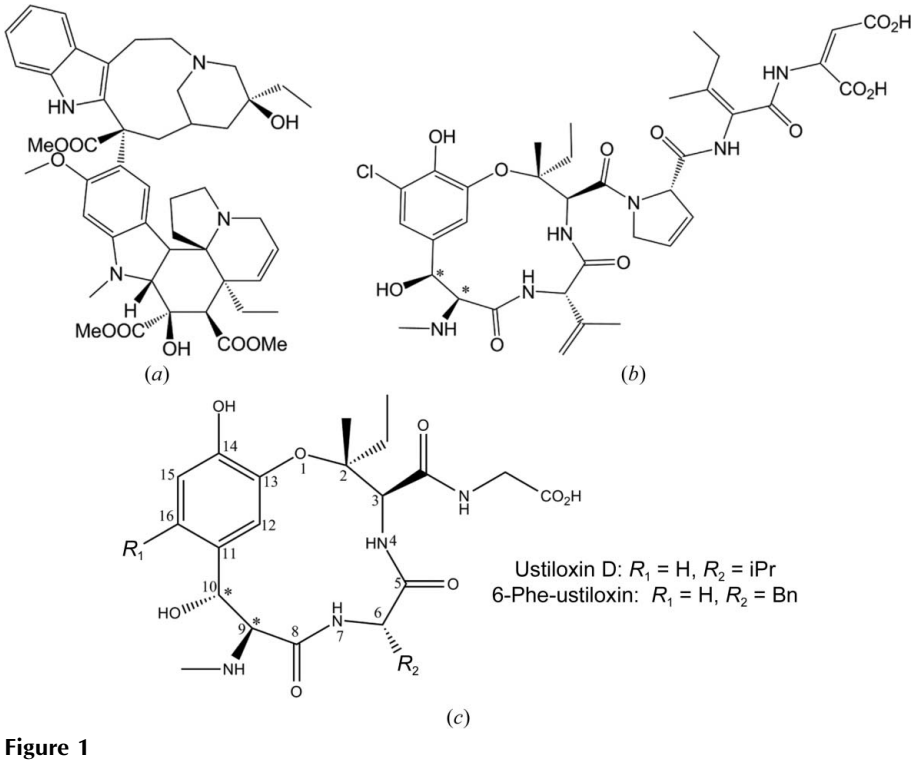

Figure 1
Chemical formulae of the vinca-domain ligands studied. (*a*) Vinblastine. (*b*) Phomopsin A. (*c*) Ustiloxins.

2.2. Crystallization and data collection

Crystals were obtained either at 277 K (T_2R) or 293 K (T_2R and sT_2R) using the hanging-drop crystallization method as described by Dorléans *et al.* (2007) and Nawrotek *et al.* (2011). In brief, T_2R crystallized at pH 7.5 using a solution consisting of 4–7%(*w*/*v*) PEG 20 000, 5%(*v*/*v*) PEG 400 and 10%(*v*/*v*) ethylene glycol as precipitants. sT_2R was crystallized at pH 6.8 using a

mixture consisting of 20–25%(*w*/*v*) PEG 1500 and 0.3–0.4 *M* Li_2SO_4 as precipitant. Crystals grew to their maximal dimensions within a week. The binding of three vinca-domain ligands, ustiloxin D, 6-Phe-ustiloxin [a modified ustiloxin D in which the isopropyl group (iPr) at position 6 is substituted by a benzyl group; Fig. 1*c*] and vinblastine, has been studied using these two crystal forms.

Ustiloxin D and 6-Phe-ustiloxin were synthesized as described by Li *et al.* (2008); vinblastine was purchased from Sigma. The crystals were soaked with one of the three ligands at 1 m*M* concentration for 24–48 h, a compromise between ligand occupancy and the resolution limit of the diffraction. Ustiloxin D was soaked into crystals of sT_2R grown from colchicine-bound tubulin [$s(Tc)_2R$]. Glycerol [at ∼20%(*v*/*v*)] was added to the sT_2R crystal soaking solution for cryoprotection. In the case of T_2R, the cryoprotectant was ethylene glycol (25%). The crystals were then flash-cooled in liquid nitrogen for diffraction data collection. Diffraction data were collected at 100 K using a Quantum ADSC 315R detector on the PROXIMA 1 beamline at SOLEIL, St Aubin, France; the wavelength was 0.98 Å. The data were integrated using *XDS* (Kabsch, 2010) and intensities were scaled and merged using *SCALA* (Winn *et al.*, 2011).

2.3. Structure refinement

The previously determined structures of sT_2R (PDB entry 3ryc; Nawrotek *et al.*, 2011) and of T_2R (PDB entry 1sa0; Ravelli *et al.*, 2004) were refined using *BUSTER* (Bricogne *et al.*, 2009). Since soaking with ligands slightly affected the isomorphism, rigid-body refinement was performed before coordinates and temperature factors were refined. Four groups of atoms comprised of each tubulin subunit and the nearest RB3 residues were defined as TLS groups; once located in the electron-density maps, the ligands were included in the TLS group of the tubulin β-subunit that contributed residues to the vinca domain. Models were visualized and manually corrected to match the electron-density maps using *Coot* (Emsley & Cowtan, 2004). The initial models of ustiloxins were derived from that of phomopsin A (Cormier *et al.*, 2008) and were idealized using the *PRODRG* server (Schüttelkopf & van Aalten, 2004).

Three structures were determined at low resolution and one at higher resolution. Difference electron-density maps revealed that 6-Phe-ustiloxin did not bind to the vinca domain of sT_2R, but was detected at the inter-heterodimeric interface of T_2R. Indeed, the difference electron-density map displayed its highest positive peak at this site (8.2σ), with the first peak height at a different location being 5.4σ. The 6-Phe-ustiloxin location is clear (Supplementary Fig. 1*a*[1]), but because of the limited resolution of the data (4.4 Å) no definite information could be obtained on its orientation or conformation in the vinca domain. Likewise, difference maps calculated from ustiloxin D-soaked T_2R crystals displayed a strong positive density peak at the vinca domain, but the resolution (4.2 Å) did not allow us to position the ligand unambiguously. Finally, soaking sT_2R crystals with vinblastine led to some resolution improvement (3.5 Å) over the 4.1 Å resolution of the known structure of T_2R–vinblastine. The electron-density maps showed that the vinblastine occupancy in sT_2R is close to 1 (Supplementary Fig. 1*b*[1]) and the structural analysis confirmed the conclusions drawn from the previous lower resolution structure. In contrast, sT_2R crystals soaked with ustiloxin D diffracted to 2.7 Å resolution (Table 1) and the corresponding difference electron-density maps allowed us to position the ligand with confidence (see §3). sT_2R-liganded structures were refined and the resulting atomic models, which have been deposited in the PDB (accession codes 3ut5 for ustiloxin D and 4eb6 for vinblastine), are of the quality expected at these resolutions (Table 1). Figures were generated with *PyMOL* (DeLano, 2002).

2.4. Determination of ligand affinities for the vinca domain

To determine their affinities for the vinca domain in $(Tc)_2R$, the effects of ustiloxin D and 6-Phe-ustiloxin on the GTPase activity of the complex were evaluated by quantifying the release of free inorganic phosphate from [γ-^{32}P]-GTP during a 24 min time course, as described by Cormier *et al.* (2008) and Wang *et al.* (2007), and the results were interpreted in terms of ligand binding. To evaluate tubulin aggregation, tubulin (at 10 μM) was incubated with vinca-domain ligands (at concentrations of 50 or 500 μM) at room temperature for 30 min in 20 m*M* potassium PIPES buffer pH 6.8. After high-speed centrifugation (80 000 rev min^{-1} in a TLA-120.1 Beckman rotor for 15 min), the supernatant and pellet were analyzed by SDS–PAGE.

3. Results

3.1. The ustiloxin D binding site

The ustiloxin D binding site was identified by inspection of difference electron-density maps calculated using diffraction data from ustiloxin-soaked sT_2R crystals. The resolution limit (2.7 Å) represents a significant improvement compared with that (3.8 Å at best) of known structures of complexes of tubulin with vinca-domain ligands (Cormier *et al.*, 2008; Gigant *et al.*, 2005). Data-collection and refinement statistics are given in Table 1. The difference density map calculated using a protein-only model clearly defined the 13-membered macrocycle of the ligand at the interface between the β- and α-tubulin subunits of the two different heterodimers in sT_2R (Fig. 2*a*), with an appendage indicating the position of the ustiloxin C-terminal glycine residue (Fig. 2*b*). Two orientations of the ligand could be fitted in the electron density, but only one had a conformation corresponding to that of the atropisomer synthesized (Li *et al.*, 2008). Refinement positioned the ligand in a manner similar to phomopsin A (Cormier *et al.*, 2008). Thus, the interactions of ustiloxin D with tubulin resemble those reported for phomopsin A, but because of the improved resolution the tubulin residues that

[1] Supplementary material has been deposited in the IUCr electronic archive (Reference: XB5051). Services for accessing this material are described at the back of the journal.

Table 1
Data-collection and refinement statistics.

Values in parentheses are for the highest resolution shell.

Crystallized complex	sT_2R	sT_2R	T_2R	T_2R
Ligand	Ustiloxin D†	Vinblastine†	Ustiloxin D	6-Phe-ustiloxin
Space group	$P2_12_12_1$	$P2_12_12_1$	$P6_5$	$P6_5$
Data-collection statistics				
Unit-cell parameters (Å)	a = 64.8, b = 128.8, c = 254.8	a = 64.7, b = 129.7, c = 252.8	$a = b$ = 328.7, c = 54.4	$a = b$ = 327.9, c = 54.5
Resolution (Å)	43.0–2.73 (2.87–2.73)	43.23–3.47 (3.65–3.47)	34.77–4.20 (4.43–4.20)	34.69–4.40 (4.64–4.40)
$\langle I/\sigma(I)\rangle$	14.8 (1.7)‡	12.2 (1.8)	13.5 (3.3)	14.6 (2.6)
Unique reflections	56466 (6803)	28253 (4025)	24048 (3517)	21984 (3201)
Multiplicity	7.5 (3.0)	3.6 (3.7)	4.1 (4.1)	4.0 (4.1)
Completeness (%)	97.3 (81.7)	99.2 (98.7)	94.6 (97.0)	99.7 (100.0)
R_{merge}§ (%)	10.2 (56.8)	7.5 (68.5)	6.8 (49.3)	5.1 (56.2)
Refinement statistics				
Resolution range (Å)	38.26–2.73	43.06–3.47	33.94–4.20	32.89–4.40
R/R_{free}¶ (%)	18.6/22.2	18.7/25.0	22.87/29.68	22.7/25.9
Coordinate error†† (Å)	0.45	1.05	0.971	1.117
B factor (Å^2)				
Protein	94.4	174.1	129.6	167.6
Nucleotide/Mg^{2+}/ligands	76.4	151.7	132.6	125.5
Water/SO_4^{2-}	86.2	158.1		
R.m.s.d. from ideal values (Engh & Huber, 2001)				
Bond lengths (Å)	0.009	0.010	0.008	0.008
Bond angles (°)	1.25	1.39	1.17	1.13
Ramachandran statistics (Chen *et al.*, 2010)				
Preferred regions (%)	95.2	87.6	83.87	92.7
Outliers (%)	1.1	2.7	6.49	3.4

† Models deposited in the PDB (accession codes 3ut5 and 4eb6 for ustiloxin D and vinblastine, respectively). ‡ The resolution limit is 2.9 Å when the last shell is such that $\langle I/\sigma(I)\rangle = 2$. § $R_{merge} = \sum_{hkl}\sum_i |I_i(hkl) - \langle I(hkl)\rangle|/\sum_{hkl}\sum_i I_i(hkl)$, where $I_i(hkl)$ is the ith used observation for unique hkl and $\langle I(hkl)\rangle$ is the mean intensity for unique hkl. ¶ $R = \sum_{hkl}\big||F_{obs}| - |F_{calc}|\big|/\sum_{hkl}|F_{obs}|$, where F_{obs} and F_{calc} are the observed and calculated structure factors, respectively. R_{free} is calculated using a subset (5%) of the data excluded from the refinement. †† Estimated from Luzzati plots.

contact the ligand are clearly defined (Figs. 2*c* and 2*d*), whereas in previous structures these interactions had to be described mostly in terms of tubulin secondary-structure elements.

On the β-tubulin side, the ustiloxin tyrosine phenolic hydroxyl points towards the H6–H7 loop (for the nomenclature of tubulin secondary-structure elements, see Nogales *et al.*, 1998) and establishes a hydrogen bond to the Proβ222 main-chain carbonyl. The ethyl end of the ligand β-hydroxyisoleucine stacks with the Tyrβ224 side chain, which is stacked with the GDP base on its other side. Finally, in the T5 loop, the β177–β181 peptide adopts the 'out' conformation which is favoured by the GTP γ-phosphate in solvent-exposed β-tubulin (Nawrotek *et al.*, 2011) and results in the Aspβ179 side chain being directed towards the solvent. In the presence of ustiloxin D, this 'out' conformation is favoured as Aspβ179 hydrogen bonds to the *N*-methylamino group of the ligand. On the α-tubulin side, the ligand induces a displacement of H10 away from the other heterodimer compared with the 'empty' vinca-domain structure (Nawrotek *et al.*, 2011); the displacement is maximal at the C-terminal end of H10 (the displacement at Argα339 C^α is 5 Å). In this helix, the Asnα329 side chain hydrogen bonds to the main-chain amide and carbonyl of the valine of ustiloxin D. In addition, residues in H10 (Proα325 and Valα328) and β-strand S9 (Valα353 and Ileα355) contribute to a hydrophobic pocket that accommodates the valine side chain of ustiloxin D. In other structures of vinca-domain ligands complexed with T_2R, α-tubulin H10 is also displaced, suggesting that its mobility, which has been noted previously (Nogales & Wang, 2006), is used to optimize the interaction between this α-tubulin hydrophobic pocket and the indole moiety of vinblastine (Gigant *et al.*, 2005), the isopropenyl group of phomopsin A (Cormier *et al.*, 2008) or the valine of ustiloxin D (this work).

The movement of α-tubulin H10 is accompanied by a reorientation of the intermediate domain. This domain is the smaller of the two globular domains that constitute a tubulin subunit; the larger one comprises the N-terminal nucleotide-binding domain together with a C-terminal helical hairpin (Nogales *et al.*, 1998). The intermediate domain consists of a central four-stranded β-sheet (S7–S10) flanked by three α-helices (H8, H9 and H10). On binding ustiloxin D the β-sheet and helix H9 rotate as a whole by 6.5° compared with the structure in the empty vinca domain sT_2R [Nawrotek *et al.*, 2011; the root-mean-square deviation (r.m.s.d.) of 50 C^α positions after this rotation is 0.56 Å, compared with 1.58 Å before]. H8 does not follow this movement; it is wedged in the α–β interface, which may restrict its position (Dorléans *et al.*, 2009). We find that the orientations of the intermediate domain of α-tubulin in the vinca domain are identical in all liganded vinca domains (this work; Cormier *et al.*, 2008; Gigant *et al.*, 2005) and in T_2R (Ravelli *et al.*, 2004), but differ from the orientation in sT_2R when the vinca domain is unliganded (Nawrotek *et al.*, 2011). Therefore, this last orientation seems to be specific to the particular crystal form obtained in this case and is changed to allow ligand binding.

3.2. Structure–function relationships of ligands similar to ustiloxin D

The effects of compounds analogous to ustiloxin D as well as that of the structurally similar peptide phomopsin A on the polymerization of purified tubulin have been investigated (Joullié *et al.*, 2011; Tonsing *et al.*, 1984). It appears from the experiments with ustiloxins that the inhibition of microtubule assembly shows a tolerance for variations at position 6 of the ustiloxin macrocycle (Fig. 1). One of the most active compounds is ustiloxin D and substitution of the valine side chain by that of phenylalanine results in a much less active compound (Li *et al.*, 2008). In order to provide a quantitative evaluation of the affinity of ustiloxin analogues for the vinca domain, we measured their inhibition of the GTPase activity of the complex of two colchicine-liganded tubulins with the stathmin-like domain of the protein RB3 [$(Tc)_2R$] in solution (Fig. 3*a*). GTP hydrolysis by $(Tc)_2R$ is a consequence of α-tubulin residues being properly positioned to enhance hydrolysis of the β-tubulin nucleotide located at the inter-heterodimeric interface in the complex. Inhibition of the $(Tc)_2R$ GTPase, which specifically measures the interference of ligands with the assembled α- and β-subunits of two different heterodimers, provides a convenient way to measure binding to the vinca domain. Rate variation is perfectly accounted for by the binding of one inhibitor to $(Tc)_2R$. The corresponding equilibrium dissociation constant of 6-Phe-ustiloxin (K_d = 12 $\pm$ 1 μM) is close to one order of magnitude larger than that of ustiloxin D (K_d = 1.8 $\pm$ 0.6 μM). Related to this, 6-Phe-ustiloxin does not favour the formation of tubulin isodesmic assemblies to the same extent as other vinca-domain ligands. This was checked using a spin-down assay, which clearly demonstrated tubulin assembly in the presence of 50 μM vinblastine or 50 μM ustiloxin D but not in the presence of the same concentration of 6-Phe-ustiloxin. Very limited tubulin assembly was nevertheless observed in the presence of a tenfold higher concentration of this ligand (Fig. 3*b*). These results are consistent with the inhibition of microtubule assembly measurements and may be rationalized in terms of the X-ray structures that we have determined.

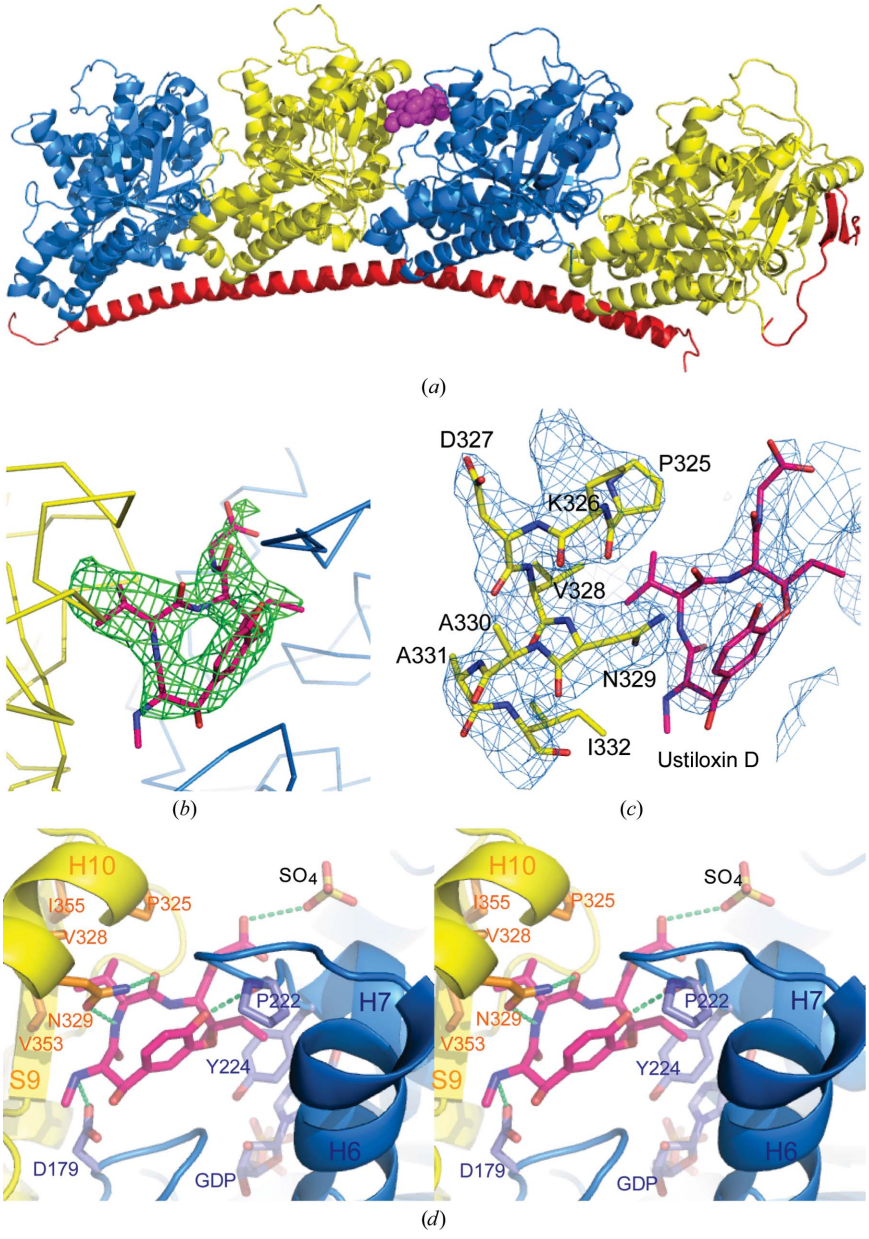

Figure 2
The vinca domain in sT_2R with bound ustiloxin D. (*a*) Overall cartoon view of sT_2R with bound ustiloxin D (in sphere mode) at the inter-heterodimeric interface. β- and α-tubulin are coloured blue and yellow, respectively, and ustiloxin D is shown in magenta. The same colour code is used in the other parts of this figure. (*b*) A stick model of ustiloxin D is overlapped with an sT_2R–ustiloxin D $F_{obs} - F_{calc}$ OMIT map contoured at the 3σ level. The traces of the polypeptide chains of β- and α-tubulin are represented. (*c*) Ustiloxin D and neighbouring residues in α-tubulin helix H10 overlapped with a $2F_{obs} - F_{calc}$ map contoured at the 1.2σ level. (*d*) Stereoview of the interactions of ustiloxin D with its environment in sT_2R.

Ustiloxin D and 6-Phe-ustiloxin only differ at position 6 of the macrocycle by the replacement of an isopropyl group by a benzyl group (Bn). The binding of this modified ligand was revealed by the 4.4 Å resolution difference electron-density maps calculated using diffraction from 6-Phe-ustiloxin-soaked T_2R crystals, after attempts to soak the more densely packed sT_2R crystals had been unsuccessful (see §2). 6-Phe-ustiloxin was modelled in such a way that its macrocycle coincided with that of ustiloxin D, with the 6-Phe side chain pointing

towards the α-subunit hydrophobic pocket surrounded by residues from H10 and S9 (see above). The lower affinity of 6-Phe-ustiloxin compared with ustiloxin D suggests that fitting 6-Phe-ustiloxin into the vinca domain embedded in T_2R involves some strain. In addition, refinement of this structural model against the crystallographic data led to ~70% ligand occupancy; this is likely to be a consequence of crystal-packing constraints that restrict the T_2R flexibility as, given the affinity of 6-Phe-ustiloxin for T_2R, one would have expected the site to be filled at the 1 m*M* concentration used for soaking.

The affinity of phomopsin A for $(Tc)_2R$ (K_d < 0.1 μ*M*; see Cormier *et al.*, 2008) is significantly higher than that of ustiloxin D. Phomopsin A mostly differs from ustiloxin D at three positions in the macrocycle: the glycine side chain at position 3 is replaced by a peptide consisting of three dehydro amino acids, the absolute configuration at position 10 is inverted and there is a chlorine substituent *ortho* to the phenolic hydroxyl group instead of the hydrogen in ustiloxin D. The effect of the last two modifications is limited. That of the chlorine is likely to be small since phomopsin B, which only differs from phomopsin A in the replacement of this atom by a hydrogen, has a similar effect on microtubule assembly (Lacey *et al.*, 1987). The effect of the absolute configuration at position 10 has also been proposed to be moderate (Li *et al.*, 2008). Indeed, in both the structures of T_2R–phomopsin A and sT_2R–ustiloxin D the hydroxyl at position 10 is in a polar environment, with the closest protein group being the Lysβ176 carbonyl or the Valβ177 amide, respectively. The major contribution to the different effects of ustiloxin D and phomopsin A on microtubule assembly is therefore likely to arise from the different substituents at position 3 of the macrocycle. A comparison of the two complex structures that we have determined shows that the side chain of phomopsin A provides more extensive interactions with the β-tubulin polypeptide chain. Interestingly, after superposition of the structures, the terminal dicarboxylate of the phomopsin A side chain is close to a conserved sulfate ion (Fig. 2*d*) originating from the crystallization buffer, which was found in all of the structures of sT_2R that we have determined so far. In the highest resolution data set, the environment of this sulfate is very well defined, showing that it makes a bidentate interaction with the guanidinium end of the Argβ278 side chain (Nawrotek *et al.*, 2011). In the T_2R–phomopsin A structure the environment of the phomopsin A carboxylates is poorly defined, probably owing to the limited resolution (4.1 Å). However, it it is likely that the dicarboxylate end of the phomopsin A side chain makes an interaction with β-tubulin similar to that of the sulfate observed at high resolution and that this interaction contributes to the higher affinity of this compound for the vinca domain and for its larger effect on microtubule assembly. More specifically, the structural data indicate that the dicarboxylate end increases the affinity of phomopsin A for the tubulin whose β-subunit is part of the vinca domain. This is consistent with the observation that in the structure of T_2R–phomopsin A one ligand is bound to the β-tubulin that is exposed to solvent and represents only part of a vinca domain (Cormier *et al.*, 2008), whereas this is not the case for ustiloxin D.

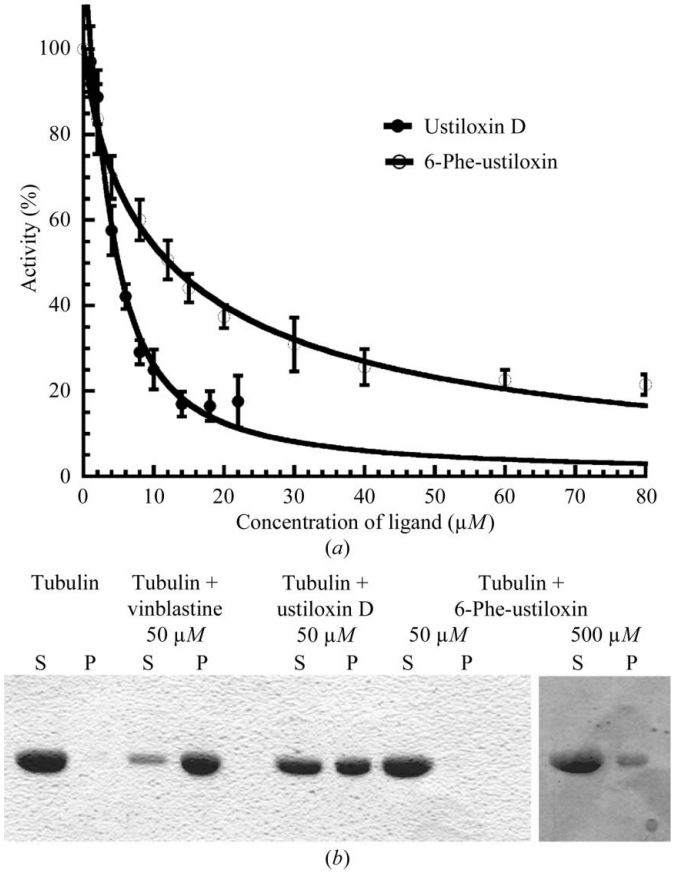

Figure 3
Binding of ustiloxin D and 6-Phe-ustiloxin to T_2R and tubulin. (*a*) Inhibition of GTPase activity. The variation in the specific GTPase activity of $(Tc)_2R$ is presented as a function of ustiloxin D (filled circles) and 6-Phe-ustiloxin (open circles) concentrations. The lines represent fits of the data calculated as described in Cormier *et al.* (2008) and Wang *et al.* (2007), from which equilibrium dissociation constants were deduced. (*b*) The variation in aggregation of tubulin (10 μ*M*) as a function of the vinca-domain ligand bound was assayed by analyzing the tubulin content in the supernatant (S) and pellet (P) after centrifugation of tubulin (used as a negative control) and of mixtures with vinblastine (used as a positive control), ustiloxin D or 6-Phe-ustiloxin at the indicated concentrations.

3.3. Adaptation of a vinca domain to different ligands is made possible by the flexibility of the arrangement of its two constitutive tubulins

We have shown previously that the arrangement of the two tubulin heterodimers in T_2R is flexible, the evidence being that it is influenced by the packing of the crystal in which it is observed (Nawrotek *et al.*, 2011). The corresponding differences may be pictured by drawing helical superassemblies of T_2R in the two known crystal forms (for the way that these assemblies are constructed, see the legend to Fig. 4). These helices have pitches of opposite sign (Fig. 4*a*), which is a consequence of the different arrangements of the two tubulins in T_2R. As the interface of the two tubulins is where vinca-domain ligands are accommodated, this observation raises the question of whether the arrangement is also influenced by

these ligands. This is indeed the case. Upon binding of ustiloxin D to sT_2R in the $P2_12_12_1$ crystal lattice, the pitch of the superhelix decreases to yield an almost circular organization (Fig. 4*a*). We also soaked the sT_2R $P2_12_12_1$ crystals with vinblastine. The resolution decreased (3.5 Å; see §2), but was sufficient to show that the relative orientation of the two tubulins was shifted towards that observed in the $P6_5$ crystal form (Fig. 4*a*). Thus, vinca-domain ligands lead the two tubulins of T_2R to adopt a relative position that favours a stable interaction with these molecules, but a comparison of structures in the $P2_12_12_1$ and $P6_5$ crystal systems shows that there is some flexibility in the inter-tubulin interface that accommodates a given compound. To evaluate this flexibility, we superimposed the β-tubulin which contributes residues to the vinca domain accommodating a given ligand in the two crystal forms, applied the same rotation to the second tubulin that constitutes the vinca domain and compared the orientations of the resulting α-subunits. In the case of ustiloxin D their orientations differ by a 7° rotation, whereas the angle is 4° in the case of vinblastine. Consistently, the superhelices built from ustiloxin D-liganded complexes in the two crystal forms differ (Fig. 4*b*) more than those built from vinblastine-liganded complexes (Fig. 4*c*).

The molecular rationale for the different superhelices is revealed by superimposing the vinca domains of complexes of vinblastine and ustiloxin D (in space group $P2_12_12_1$) using the β-subunits to define the superposition. When the interactions of vinblastine with α-tubulin residues in the ustiloxin D complex are analyzed, several clashes appear. They involve in particular the indole group of the vinblastine catharanthine moiety and Asnα329, as well as residues of the S9–H10 hydrophobic pocket (Valα328 in H10 and Valα353 in S9). An additional 5.5° rotation of the α-subunit bound to ustiloxin D superimposes it on that which accommodates vinblastine, relieves all these clashes and transforms the superhelix based on sT_2R–ustiloxin D into that based on sT_2R–vinblastine.

4. Discussion

The structure of sT_2R–ustiloxin D establishes the interactions of this ligand with tubulin at a resolution that is unprecedented for vinca-domain ligands. This information allowed us to rationalize three aspects of structure–activity data of modified ustiloxins (Li *et al.*, 2008), in addition to those that we have already discussed concerning 6-Phe-ustiloxin. Firstly, the substitution of the C14 hydroxyl by a methoxy group in the ligand drastically affects the potential of the compound to inhibit the polymerization of microtubules. This implies that the hydrogen bond observed between this hydroxyl and the Proβ222 carbonyl is crucial for proper binding of ustiloxins. Secondly, the inversion of the configuration of C9 and C10 leads to poorly active compounds. Since the inversion of configuration at C10 does not have a great effect on the activity, the modification at C9 must be important. It affects the orientation of the *N*-methylamino group and prevents the formation of a hydrogen bond with Aspβ179. Finally, comparison of the structure of sT_2R–ustiloxin D with that of T_2R–phomopsin A shows that their carboxy-terminal tails are similarly located with respect to tubulin (see above). Modified vinca alkaloids have been synthesized in which the carboxy-terminal tail of phomopsin A was incorporated (Ngo *et al.*, 2009). This addition did not lead to a greatly improved activity, probably because the ionic interaction of the terminal

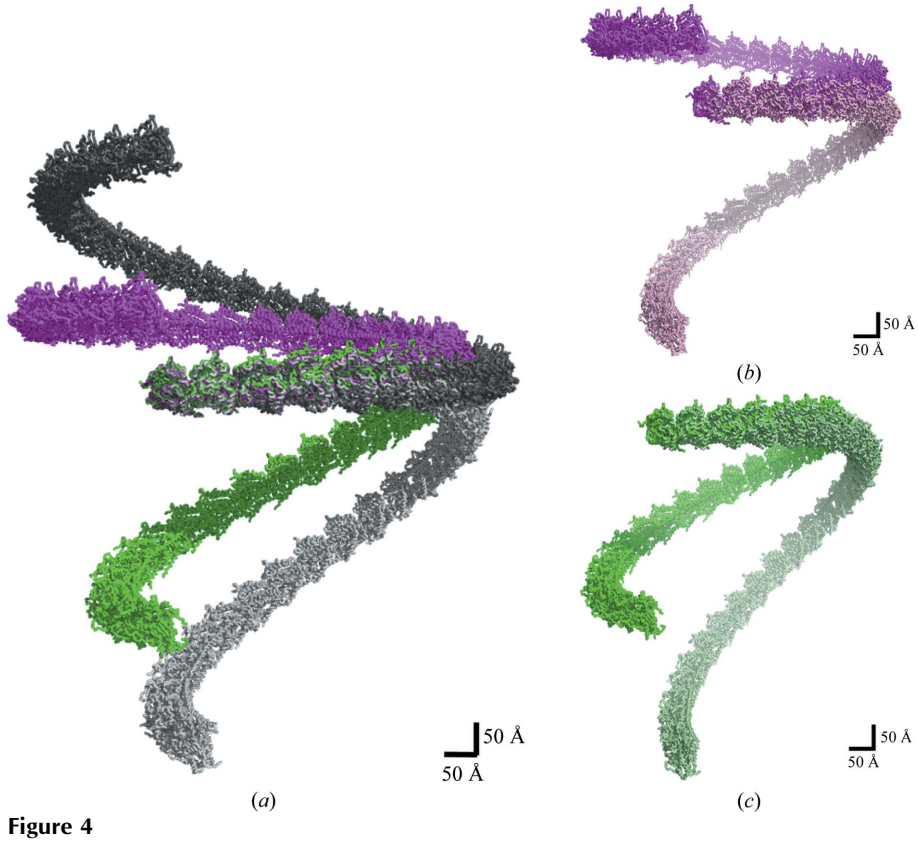

Figure 4
The effects of ustiloxin D and vinblastine on the quaternary arrangements of the tubulin heterodimers that constitute the vinca domain. (*a*) The models resulting from the repetition of nonliganded sT_2R ($P2_12_12_1$) and T_2R ($P6_5$; dark grey and light grey, respectively), sT_2R–ustiloxin D ($P2_12_12_1$; magenta) and sT_2R–vinblastine ($P2_12_12_1$; green) have been superimposed. Each was obtained by superimposing the $\alpha1\beta1$ moiety of the mth complex onto the $\alpha2\beta2$ moiety of the $(m-1)$th complex and by keeping in the final model $(\alpha1\beta1)_1$, $(\alpha2\beta2)_1$, $(\alpha2\beta2)_2$, …, $(\alpha2\beta2)_n$. The resulting helices are viewed perpendicular to their axis, highlighting the opposite signs of the pitches of the helices of nonliganded and vinblastine-liganded sT_2R. (*b*) Superimposed models resulting from the repetition of ustiloxin D complex structures in space groups $P2_12_12_1$ (sT_2R) and $P6_5$ (T_2R), as in (*a*) (dark and light magenta, respectively). (*c*) Superimposed models resulting from the repetition of vinblastine complex structures in space groups $P2_12_12_1$ (sT_2R) and $P6_5$ (T_2R), as in (*a*) (dark and light green, respectively).

carboxylates of the phomopsin A side chain with the tubulin residue Argβ278 could not be established. Our results suggest that this interaction would be made by the terminal carboxylates of the phomopsin A side chain when substituted into ustiloxin D and that this substitution would lead to a much improved activity.

Our results also provide a structural explanation of the observation that the protofilament-like assemblies formed in the presence of vinca-domain ligands are polymorphic, helices and rings being formed (Amos *et al.*, 1984; Mitra & Sept, 2004). The two tubulin heterodimers that constitute a vinca domain are arranged with respect to each other such that the repetition of this arrangement leads to the formation of a superhelix (Fig. 4). Taken together with our previous results on vinblastine (Gigant *et al.*, 2005), the results that we have obtained with ustiloxin D allow us to characterize the superhelix formed in two respects. Firstly, its pitch is a function of the ligand bound, although there is some variability for each ligand. Secondly, the range of the pitches observed includes a zero value, which corresponds to the formation of a ring. To understand how the ligand influences the pitch of the helix, we have compared the complexes of tubulin with ustiloxin D and vinblastine in the same crystal form. The pitch of the helix formed from the tubulins that bind the ligand is 2.5 times smaller in the first case than in the second (80 *versus* 200 Å) and vinblastine does not fit into the vinca domain embedded in the sT_2R–ustiloxin D structure. It is not surprising that the variable tubulin assemblies observed in the presence of different vinca-domain ligands are accounted for by different requirements for the accommodation of these ligands at the tubulin intermolecular longitudinal interface.

Diffraction data were collected at the SOLEIL synchrotron, Saint-Aubin, France. We are grateful to the machine and PROXIMA beamline groups whose efforts made these experiments possible. This work was supported by the Centre National pour la Recherche Scientifique, by the Fondation pour la Recherche Médicale (grant DEQ20081213979) and by the Agence Nationale de la Recherche (grant ANR-09-BLAN-0071). FMR was supported by an Association pour la Recherche sur le Cancer postdoctoral fellowship.

References

Amos, L. A., Jubb, J. S., Henderson, R. & Vigers, G. (1984). *J. Mol. Biol.* **178**, 711–729.
Bricogne, G., Blanc, E., Brandl, M., Flensburg, C., Keller, P., Paciorek, W., Roversi, P., Smart, O., Vonrhein, C. & Womack, T. O. (2009). *BUSTER* v.2.8.0. Cambridge: Global Phasing Ltd.
Castoldi, M. & Popov, A. V. (2003). *Protein Expr. Purif.* **32**, 83–88.
Charbaut, E., Curmi, P. A., Ozon, S., Lachkar, S., Redeker, V. & Sobel, A. (2001). *J. Biol. Chem.* **276**, 16146–16154.
Chen, V. B., Arendall, W. B., Headd, J. J., Keedy, D. A., Immormino, R. M., Kapral, G. J., Murray, L. W., Richardson, J. S. & Richardson, D. C. (2010). *Acta Cryst.* D**66**, 12–21.
Cormier, A., Marchand, M., Ravelli, R. B., Knossow, M. & Gigant, B. (2008). *EMBO Rep.* **9**, 1101–1106.
Correia, J. J., Baty, L. T. & Williams, R. C. (1987). *J. Biol. Chem.* **262**, 17278–17284.
DeLano, W. L. (2002). *PyMOL*. http://www.pymol.org.
Dorléans, A., Gigant, B., Ravelli, R. B., Mailliet, P., Mikol, V. & Knossow, M. (2009). *Proc. Natl Acad. Sci. USA*, **106**, 13775–13779.
Dorléans, A., Knossow, M. & Gigant, B. (2007). *Methods Mol. Med.* **137**, 235–243.
Emsley, P. & Cowtan, K. (2004). *Acta Cryst.* D**60**, 2126–2132.
Engh, R. A. & Huber, R. (2001). *International Tables for Crystallography*, Vol. *F*, 1st ed., edited by M. G. Rossmann & E. Arnold, pp. 382–392. Dordrecht: Kluwer Academic Publishers.
Gigant, B., Wang, C., Ravelli, R. B., Roussi, F., Steinmetz, M. O., Curmi, P. A., Sobel, A. & Knossow, M. (2005). *Nature (London)*, **435**, 519–522.
Hamel, E. (1992). *Pharmacol. Ther.* **55**, 31–51.
Hamel, E. & Covell, D. G. (2002). *Curr. Med. Chem. Anticancer Agents*, **2**, 19–53.
Joullié, M. M., Berritt, S. & Hamel, E. (2011). *Tetrahedron Lett.* **52**, 2136–2139.
Kabsch, W. (2010). *Acta Cryst.* D**66**, 125–132.
Knipling, L., Hwang, J. & Wolff, J. (1999). *Cell Motil. Cytoskeleton*, **43**, 63–71.
Koiso, Y., Natori, M., Iwasaki, S., Sato, S., Sonoda, R., Fujita, Y., Yaegashi, H. & Sato, Z. (1992). *Tetrahedron Lett.* **33**, 4157.
Lacey, E., Edgar, J. A. & Culvenor, C. C. (1987). *Biochem. Pharmacol.* **36**, 2133–2138.
Li, P., Evans, C. D., Wu, Y., Cao, B., Hamel, E. & Joullié, M. M. (2008). *J. Am. Chem. Soc.* **130**, 2351–2364.
Mitra, A. & Sept, D. (2004). *Biochemistry*, **43**, 13955–13962.
Nawrotek, A., Knossow, M. & Gigant, B. (2011). *J. Mol. Biol.* **412**, 35–42.
Ngo, Q. A., Roussi, F., Cormier, A., Thoret, S., Knossow, M., Guénard, D. & Guéritte, F. (2009). *J. Med. Chem.* **52**, 134–142.
Nogales, E., Downing, K. H., Amos, L. A. & Löwe, J. (1998). *Nature Struct. Biol.* **5**, 451–458.
Nogales, E. & Wang, H.-W. (2006). *Curr. Opin. Struct. Biol.* **16**, 221–229.
Ravelli, R. B., Gigant, B., Curmi, P. A., Jourdain, I., Lachkar, S., Sobel, A. & Knossow, M. (2004). *Nature (London)*, **428**, 198–202.
Schüttelkopf, A. W. & van Aalten, D. M. F. (2004). *Acta Cryst.* D**60**, 1355–1363.
Tonsing, E. M., Steyn, P. S., Osborn, M. & Weber, K. (1984). *Eur. J. Cell Biol.* **35**, 156–164.
Wang, C., Cormier, A., Gigant, B. & Knossow, M. (2007). *Biochemistry*, **46**, 10595–10602.
Winn, M. D. *et al.* (2011). *Acta Cryst.* D**67**, 235–242.